

Featuring work from Prof. Kelvin Sze-Yin Leung and Dr. Yingyan Huang at the Department of Chemistry, Hong Kong Baptist University, HKSAR, P.R.China.

Interactions between cerium dioxide nanoparticles and arsenite change their biological fate in the gastrointestinal tract of mice

The co-existence of engineered nanoparticles and heavy metals in the environment poses potential risk to human health. This study investigates the distinctive physiological behaviour of  $\text{CeO}_2$ -As(III) mixture in an *in vitro* gastrointestinal model, and the biological fate as well as the toxicological changes in mice.

As featured in:



See Kelvin Sze-Yin Leung *et al.*, *Environ. Sci.: Nano*, 2023, 10, 1585.



Cite this: *Environ. Sci.: Nano*, 2023, 10, 1585

## Interactions between cerium dioxide nanoparticles and arsenite change their biological fate in the gastrointestinal tract of mice†

Yingyan Huang, <sup>a</sup> Judy Tsz-Shan Lum, <sup>a</sup>  
Wai-Kit Ho <sup>b</sup> and Kelvin Sze-Yin Leung <sup>\*ac</sup>

The large-scale production of engineered nanoparticles (ENPs), such as cerium dioxide nanoparticles (CeO<sub>2</sub> NPs), raises concerns towards their impact on human health. The co-existence of ENPs and heavy metals in the natural environment is particularly worrisome because people are ingesting them. In this study, the behaviors of CeO<sub>2</sub> NPs and arsenite (As(III)) during the digestive process were first investigated using an *in vitro* gastrointestinal tract (GIT) model, and then studied in a mouse model *via* oral co-exposure. The results suggest that CeO<sub>2</sub> NPs of both 10 nm and 30 nm in diameter strongly adsorbed As(III) during the digestive process, resulting in the decreased bioaccessibility of As in the GIT fluids. Corresponding to the decreased As bioaccessibility obtained from the *in vitro* GIT model, exposure to a 10 nm CeO<sub>2</sub> NP–As(III) mixture led to a decrease in As(III) bioaccumulation in organs. However, exposure to a 30 nm CeO<sub>2</sub> NP–As(III) mixture increased the relative bioavailability of Ce and As in mice. Interestingly, toxicity enhancement was observed in the 30 nm CeO<sub>2</sub> NP–As(III) mixture exposure group, probably due to the redox reaction between Ce(IV) and As(III) taking place on the NP surface, affecting the As(III) metabolism in the liver. Our findings showed the first step in elucidating the effect of two types of pollutants increasingly found in our environment, ENPs and heavy metals, on mammalian health.

Received 20th February 2023,  
Accepted 12th April 2023

DOI: 10.1039/d3en00109a

rs.li/es-nano

### Environmental significance

The co-existence of engineered nanoparticles and heavy metals in the natural environment may be enhancing their risks to humans; we simply don't know. The increasing prevalence of both of these toxic entities means that we need to know: they are in our food and water. This is the first study to elucidate the joint effects of one type of nanoparticle, cerium dioxide nanoparticles (CeO<sub>2</sub> NPs, with diameters of 10 nm or 30 nm) and one metalloid, arsenite (As(III)), on mammals after oral uptake. We tracked their behaviors in the gastrointestinal tract (GIT), studied their biodistribution and evaluated their toxicity in mice. The results suggest that the interactions between the two selected CeO<sub>2</sub> NPs and As(III) in the simulated GIT resulted in various impacts on the physicochemical properties (zeta potential and hydrodynamic size) of NPs and bioaccessibility of As(III), leading to the altered biological fate of both after their oral co-exposure in mice.

## Introduction

With their superior physical and chemical properties, engineered nanoparticles (ENPs) are finding applications in various fields, from pharmaceuticals to semiconductors to consumer products.<sup>1</sup> The large-scale production and broad

applications of ENPs have led to their release into the environment,<sup>2–4</sup> which has raised growing concerns about their effects on the environment and, ultimately, on humans. Previous studies have evaluated and explored the toxicological mechanism of ENPs, suggesting that ENPs cause oxidative stress originating from reactive oxygen species (ROS) or reactive nitrogen species (RNS), or that they are genotoxic, damaging DNA or causing cell apoptosis.<sup>1,5,6</sup> As one of the more widely used ENPs, cerium dioxide nanoparticles (CeO<sub>2</sub> NPs) are being used as catalysts, fuel additives and abrasives.<sup>7</sup> The presence of anthropogenic CeO<sub>2</sub> NPs has been confirmed in surface waters,<sup>8–12</sup> sewage sludge<sup>13</sup> and soil.<sup>14</sup> As evidence of the concern, CeO<sub>2</sub> NPs have been included in a priority list of nanomaterials requiring urgent evaluation for their environmental safety

<sup>a</sup> Department of Chemistry, Hong Kong Baptist University, Kowloon Tong, Hong Kong Special Administrative Region, China. E-mail: s9362284@hkbu.edu.hk

<sup>b</sup> Department of Applied Biology and Chemical Technology, The Hong Kong Polytechnic University, Hung Hom, Hong Kong Special Administrative Region, China

<sup>c</sup> HKBU Institute of Research and Continuing Education, Shenzhen Virtual University Park, Shenzhen, China

† Electronic supplementary information (ESI) available. See DOI: <https://doi.org/10.1039/d3en00109a>



and human health impact by the Organization for Economic Cooperation and Development (OECD).<sup>15</sup> Therefore, immediate attention should be paid to the fate and ecological implications of CeO<sub>2</sub> NPs in the natural environment.

In a natural environment, ENPs inevitably co-exist with other pollutants, such as heavy metals (HMs).<sup>16</sup> Due to the large surface-to-volume ratio and high surface reactivity of ENPs, the co-existing HMs will be easily adsorbed onto the ENPs and interact with them; this phenomenon is known as multi-contaminant interaction. Living organisms are a third factor (actor) in this scenario. HMs can change the fate of ENPs in organisms, and *vice versa*. For instance, in a study of overweight mice orally co-exposed to ZnO NPs and Pb(II), Jia *et al.*<sup>17</sup> reported significant accumulation of both elements (Zn and Pb) in the mouse kidney, while there was greater deposition of Pb(II) in the liver, spleen, lung and heart of mice, apparently due to the presence of ZnO NPs. The increased Pb levels in major organs induced liver injury in these mice. Teng *et al.*<sup>18</sup> observed that the oral co-exposure of pregnant mice to ZnO NPs and Cd(II) increased maternal-fetal transfer of both, resulting in embryotoxicity. After intraperitoneal injection of silica nanoparticles (SiNPs) and Cd(II) into mice, SiNPs significantly enhanced Cd accumulation in their kidney and liver, leading to synergistic toxicity observed in the co-exposure group.<sup>19</sup> However, these previous studies did not elucidate the interactions between ENPs and HMs in biological systems. Understanding the chemical interactions could help us better understand the toxicological consequences of these contaminants in actual environments.

Currently, water treatment facilities are not equipped to remove ENPs. For example, CeO<sub>2</sub> NPs were found to be reduced by less than 5% from source water to finished drinking water.<sup>20</sup> The presence of HMs in drinking water, particularly in developing countries, has been reported in past studies.<sup>21</sup> Thus, oral exposure to both ENPs and HMs is increasing likely for humans, and the risks posed by this exposure cannot be underestimated.<sup>22,23</sup> After being ingested by a person, ENPs and HMs pass through the gastrointestinal tract (GIT). During this passage, the chemical environment differs enormously: from the oral cavity to the stomach to the intestine. These different environments might affect the adsorption of HMs onto ENPs as well as the interaction between them. The impact originating from this adsorption or interaction on the bioaccessibility of HMs in the GIT has not been studied. Although it is difficult to investigate the behaviors of ENPs and HMs in the GIT in the human body, a well-established *in vitro* GIT model provides an alternative. The model is composed of a series of complex mixtures of salts and enzymes as simulated gastrointestinal fluids (sGIFs) including saliva and gastric and intestinal juices.<sup>24,25</sup>

Compared with other ENPs, the uniqueness of CeO<sub>2</sub> NPs lies in their ability to change between the two oxidation states, Ce(III) and Ce(IV), on the NP surface, which gives them remarkable redox activity. Among the HMs, metalloid arsenic (As) is classified as a class I human carcinogen by the

International Agency for Research on Cancer (IARC). More than 230 million people are suffering from As contamination in food or water around the world.<sup>26</sup> Furthermore, As in natural environments occurs as two predominant species: inorganic trivalent arsenite (As(III)) and inorganic pentavalent arsenate (As(V)).<sup>27</sup> Previous studies reported that the interaction between CeO<sub>2</sub> NPs and As alters the CeO<sub>2</sub> NP surface reactivity<sup>28</sup> as well as their behavior and oxidation state<sup>29</sup> in water, and may ultimately affect toxicity. It is possible that more detrimental effects can be provoked as compared to the exposure to individual constituents.

Given these implications, the joint effects of CeO<sub>2</sub> NPs and As(III) on humans after oral uptake may result from both their bioaccessibility and their interactions during the digestive process. However, none of the previous studies have explored the linkage between the behaviors of CeO<sub>2</sub> NPs in the GIT and their biological fate in humans after the oral co-exposure.

Specifically in this study, we firstly investigated the adsorption of As(III) onto CeO<sub>2</sub> NPs and the alteration of NP physicochemical properties as a result of the interaction between them during digestion. An *in vitro* GIT model was used to mimic the digestive process. The joint effects of CeO<sub>2</sub> NPs and As(III) were then investigated in mice. As the size of CeO<sub>2</sub> NPs affects their toxicity,<sup>30</sup> we included two different sizes of CeO<sub>2</sub> NPs, 10 nm and 30 nm. The results of this study are the first report of the interaction between CeO<sub>2</sub> NPs and As(III) in sGIFs. The alteration of the physicochemical properties of NPs as a result of the interaction is an important part of the biological fate of CeO<sub>2</sub> NPs and As(III) in mammals that have been exposed to them orally.

## Materials and methods

### Chemicals and reagents

Sodium chloride (NaCl) (ACS reagent, ≥99.0%), anhydrous sodium sulfate (Na<sub>2</sub>SO<sub>4</sub>) (≥99%), sodium bicarbonate (NaHCO<sub>3</sub>) (ACS reagent, ≥99.7%), potassium phosphate monobasic (KH<sub>2</sub>PO<sub>4</sub>) (ACS reagent, ≥99.0%), uric acid (≥99%, crystalline), urea (ACS reagent, 99.0–100.5%), α-amylase from porcine pancreas (type VI-B, ≥5 units per mg solid), mucin from porcine stomach (type II), pepsin from porcine gastric mucosa (powder, ≥250 units per mg solid), bile from bovine and ovine (bile acid mixture), pancreatin from porcine pancreas (8 × USP specifications) and trypsin from bovine pancreas (type I, ~10 000 BAEE units per mg protein) were obtained from Sigma-Aldrich (MO, USA). Magnesium chloride hexahydrate (99%, for biochemistry) and ammonium bicarbonate (99%, for analysis) were purchased from Acros Organics (NJ, USA). Potassium chloride (KCl) (99.5–101.0%) and trace-metal grade nitric acid (HNO<sub>3</sub>, 67–69%) were purchased from AnalAR NORMAPUR® (VWR Chemicals, PA, USA). Anhydrous calcium chloride (CaCl<sub>2</sub>) was obtained from Panreac Química SA (Spain). Sodium (*meta*) arsenite (NaAsO<sub>2</sub>) (≥96%) and sodium arsenate dibasic heptahydrate (Na<sub>2</sub>HAsO<sub>4</sub>·7H<sub>2</sub>O) (≥98%) were obtained from



Sigma-Aldrich. Hydrogen peroxide ( $\text{H}_2\text{O}_2$ , 30% w/w) was purchased from Fisher BioReagents (Thermo Fisher Scientific, CA, USA). Commercialized  $\text{CeO}_2$  NPs with 30–50 nm nominal diameter (referred to here as 30 nm  $\text{CeO}_2$  NPs) and 10 nm diameter (referred to here as 10 nm  $\text{CeO}_2$  NPs) were purchased from US Research Nanomaterials, Inc. (TX, USA) and Meliorum Technologies (NY, USA), respectively. Standard monomethylarsonic acid (MMA) and dimethylarsinic acid (DMA) with purity >95% were obtained from FUJIFILM Wako Pure Chemical Industries, Ltd. (Osaka, Japan). Standard solutions of Ce, As and rhodium (Rh) were prepared by appropriate dilution of the corresponding 1000  $\text{mg L}^{-1}$  stock solutions (High-Purity Standards, Charleston, SC, USA). Ultrapure water (18.2  $\text{M}\Omega$  cm, Millipore, MA, USA) generated from a Milli-Q® Reference A+ system was used for the preparation of all solutions.

### Adsorption of As(III) on $\text{CeO}_2$ NPs in UPW and sGIFs

30 nm and 10 nm  $\text{CeO}_2$  NP solutions were prepared at a concentration of 12 000  $\text{mg L}^{-1}$  from dilution of the stock solution with UPW. An As(III) working solution was prepared at a concentration of 368  $\text{mg L}^{-1}$  by dissolving a  $\text{NaAsO}_2$  solid in UPW. The As(III) solution was added to a solution containing 3000  $\text{mg L}^{-1}$   $\text{CeO}_2$  NPs to obtain six final elemental concentrations of As(III) (0, 9.2, 18.4, 23, 36.8, 46 and 92  $\text{mg L}^{-1}$ , referred to as Lev 0, Lev 1, Lev 2, Lev 3, Lev 4, Lev 5 and Lev 6, respectively, in the following discussion). The *in vitro* GIT model used in this study was modified from DIN 19738 and has been used in previous studies.<sup>24,25</sup> This simulated GIT model consists of three phases of sGIFs, mimicking saliva, gastric and intestinal juices. The composition of the sGIFs as well as the corresponding incubation conditions are listed in Fig. S1.† More details about the procedures are described in the ESI.† The dilution factors for phase 2 (gastric juice) and phase 3 (intestinal juice) with respect to phase 1 (saliva) were 3.33× and 6.66×, respectively.

The concentrations of  $\text{CeO}_2$  NPs and As(III) (including the As(III) dissolved in solution and As(III) adsorbed onto NPs) in the saliva, gastric and intestinal mixture were determined after microwave-assisted acid digestion of samples taken out from each step. To separate the As(III) dissolved in the solution from As(III) adsorbed onto  $\text{CeO}_2$  NPs, 500  $\mu\text{L}$  of the mixture taken out from each step was centrifuged for 30 min at 14 000g at 22 °C (Eppendorf 5430R, Hamburg, Germany). The supernatant was decanted and diluted with 2%  $\text{HNO}_3$ . Rh was added into the diluted supernatant as an internal standard. The diluted supernatant was introduced into an ICP-MS (Agilent 7900, Santa Clara, CA, USA) directly for the quantification of As and Ce, which was regarded as the dissolved As and dissolved Ce ions. The adsorption capacity ( $q_t$ ,  $\text{mg g}^{-1}$ ), which refers to As(III) adsorbed onto  $\text{CeO}_2$  NPs, was calculated using eqn (1):

$$q_t = \frac{(C_0 - C_t)V}{m} \quad (1)$$

where  $C_0$  is the total concentration of As(III) in the mixture ( $\text{mg L}^{-1}$ ),  $C_t$  is the concentration of As(III) dissolved in the mixture after the corresponding incubation time in saliva and gastric and intestinal juices ( $\text{mg L}^{-1}$ ),  $V$  (L) is the volume of the solution, and  $m$  (g) is the mass of  $\text{CeO}_2$  NPs in the mixture.

The bioaccessibility of As in each phase was calculated as follows:

$$\begin{aligned} \text{Bioaccessibility (\%)} & \quad (2) \\ & = \frac{\text{arsenic in collected supernatant (mg)}}{\text{total arsenic in matrix (mg)}} \times 100\% \end{aligned}$$

To compare the effect of sGIFs on the adsorption of As onto  $\text{CeO}_2$  NPs, the adsorption of As(III) on  $\text{CeO}_2$  NPs was also assessed in UPW under similar conditions (*i.e.* similar incubation time, incubation temperature and experimental procedures with pH adjustment in UPW in each phase); the procedures are shown in Fig. S2.† For incubation times, the phases corresponding to the saliva, gastric juice and intestinal juice in the case of UPW were defined as 5 min in UPW, additional 2 h in UPW and additional 4 h in UPW. The pH was adjusted in each phase with HCl or NaOH. The term 'UPW' will be referred to as pH adjusted UPW in all discussions. The operational parameters for ICP-MS analysis are shown in Table S1.†

### Characterization of $\text{CeO}_2$ NPs

The morphology of pristine  $\text{CeO}_2$  NPs was characterized using a transmission electron microscope (TEM, JEOL JEM-2100F, Japan) (Fig. S3.†). Solutions were taken out after each phase in the *in vitro* GIT model (or each specific incubation time in the case of UPW as a control) in cases of Lev 0 and Lev 6, for the hydrodynamic diameter ( $D_H$ ) and zeta potential measurement of NPs using a Zetasizer Nano-ZS system (dynamic light scattering, DLS) (Malvern Instruments Ltd., UK). X-ray photoelectron spectroscopy (XPS, SKL-12 spectrometer modified with a VG CLAM 4 multichannel hemispherical analyzer) was used to determine the content of Ce(III) and Ce(IV) on the surface of  $\text{CeO}_2$  NPs.

### Animal study

Twenty-four eight-week-old male ICR mice were purchased from Laboratory Animal Service Center (The Chinese University of Hong Kong, Hong Kong). All mice were housed in cages under conditions of 22 °C, 40–70% humidity and a 12:12 h light/dark cycle, where they had free access to food and water. They were first acclimatized for two weeks prior to any experiments. Afterwards, they were randomly divided into six groups of four mice each. They were exposed to UPW, 30 nm  $\text{CeO}_2$  NPs (15  $\text{mg kg}^{-1}$ ), 10 nm  $\text{CeO}_2$  NPs (15  $\text{mg kg}^{-1}$ ), and As(III) (0.46  $\text{mg kg}^{-1}$ ) or co-exposed to 30 nm  $\text{CeO}_2$  NPs + As(III) (15 + 0.46  $\text{mg kg}^{-1}$ ) and 10 nm  $\text{CeO}_2$  NPs + As(III) (15 + 0.46  $\text{mg kg}^{-1}$ ) by oral gavage once per two days for 30 days. The concentration of  $\text{CeO}_2$  NPs or As(III) in the dosed solution



was equivalent to that in simulated saliva in the case of Lev 6 in the *in vitro* GIT model. The body weight of each mouse was recorded each week. On day 31, the mice were weighed and sacrificed by cervical dislocation. Blood was collected by cardiac puncture and was stored in tubes containing an anti-coagulant (EDTA). Plasma was obtained as a supernatant after the centrifugation of blood (1000g, 4 °C, 10 min) and was stored at -80 °C. The entire kidney, liver, spleen, brain and bladder were weighed individually, and then washed with cold phosphate buffer saline. The liver was divided into three parts for elemental analysis, toxicity analysis and pathological observation. All the collected organs were stored at -80 °C before analysis. All animal procedures were performed in accordance with the Guidelines for Care and Use of Laboratory Animals of Hong Kong Baptist University and approved by the Animal Ethics Committee of Hong Kong Baptist University (Reference No.: REC/19-20/0367).

### Histopathological examination of tissue

Liver tissues were fixed with 4% paraformaldehyde solution at 4 °C for 3 d and then were dehydrated by a series of 30–100% ethanol solutions, a 1:1 (v/v) ethanol/xylene substitute mixture and a xylene substitute. Afterwards, the tissues were infiltrated in paraffin at 60 °C for 2 d and finally fixed in paraffin at room temperature. Then the paraffin-embedded tissues were sectioned with a microtome (Leica Biosystems, Germany) into 5 µm-thick sections, followed by hematoxylin and eosin (H & E) staining for histological examination. The histopathological examination was conducted using a bright field microscope (Olympus, CKX53 culture microscope, Japan).

### Quantification of Ce and total As (tAs) in tissues

The collected organs (liver, spleen, kidney, bladder, and brain) were homogenized using a ceramic mortar with the aid of liquid nitrogen (LN<sub>2</sub>). Afterwards, an accurately weighed mass of an organ was then digested by microwave-assisted acid digestion with trace-metal grade HNO<sub>3</sub> and H<sub>2</sub>O<sub>2</sub>. The digested solution was diluted to 10 mL after addition of Rh as an internal standard, and then Ce as well as tAs was quantified using ICP-MS. External calibration curves (the calibration standard range for Ce and As was 0–100 µg L<sup>-1</sup> and 0–50 µg L<sup>-1</sup>, respectively) from standard solutions of ionic As and Ce were applied. The operational parameters for ICP-MS are shown in Table S1.†

The relative bioavailability of Ce or As was determined as follows:

$$\text{Relative bioavailability of Ce (\%)} = \frac{[\text{Ce}]_{\text{mice}}}{\text{Ce dose}} \times 10000 \quad (3)$$

$$\text{Relative bioavailability of As (\%)} = \frac{[\text{As}]_{\text{mice}}}{\text{As dose}} \times 100 \quad (4)$$

where [Ce]<sub>mice</sub> is the sum of Ce concentrations in the mouse liver, spleen and kidney (ng g<sup>-1</sup>); [As]<sub>mice</sub> is the sum of As

concentrations in the mouse liver, bladder, brain, spleen and kidney (ng g<sup>-1</sup>); the Ce dose and As dose are the total Ce or As dosing levels during the exposure period (ng g<sup>-1</sup>). The factor “10 000×” was used in the case of Ce for comparison due to the low adsorption of Ce in mice.

### Speciation of As species in the liver

The extractable As species (As(III), As(V), MMA and DMA) were measured by HPLC-ICP-MS (Agilent 1260 Infinity II, Agilent 8900 ICP-QQQ, Santa Clara, CA, USA), and ICP-MS was operated in collision cell mode using helium as the cell gas. The chromatograph was equipped with a standard autosampler, a degasser and an anion exchange column (Hamilton PRP X-100, 5 µm, 4.6 × 250 mm). A gradient elution was applied, as shown in Table S2.†

The method for extracting As species from the liver was modified based on the method reported in previous studies.<sup>31,32</sup> Briefly, the homogenized liver tissues were extracted with ultrapure water (1:10, v/v). The extraction was facilitated by continuous vortex mixing for 30 s followed by ultrasonication on ice for 15 min. The mixture was centrifuged (12 000 rpm, 4 °C, 15 min) and the supernatant was diluted 2-fold. The diluted supernatant was filtered through a 0.22 µm nylon syringe filter prior to injection into the HPLC system. The qualification and quantification of the four As species was done using external calibration curves from As(III), As(V), MMA and DMA standards (calibration points: 0, 0.2, 0.5, 1, 2, 5, 10, 20 µg L<sup>-1</sup>). The unknown As species (uAs) was defined as the difference between the tAs determined by ICP-MS and the four detected As species contents measured by HPLC-ICP-MS. The operational parameters for the HPLC-ICP-MS are shown in Table S2.†

For quality control, the recoveries and standard deviations of tAs and the four As species were studied by spiking As(III), As(V), MMA and DMA into the homogenized liver tissues collected from the control group. Triplicate analyses were performed. The recoveries of the extraction are shown in Table S3.† all of which were satisfactory. The limit of detection (LOD) and limit of quantification (LOQ) are shown in Table S3.†

### Biochemical analysis

Creatine in the plasma collected was determined using a commercial kit based on the Jaffe reaction (Cayman Chemical, MI, USA). Lactate dehydrogenase (LDH) and alanine aminotransferase (ALT) were also determined using commercial kits provided by BioAssay System (Hayward, CA).

### Measurement of the oxidative stress and inflammation biomarkers in the mouse liver

The oxidative stress in the mouse liver was evaluated using superoxide dismutase (SOD) by a commercial kit (Cayman Chemical, MI, USA). The concentrations of tumor necrosis factor-α (TNF-α) and interleukin-1β (IL-1β), which are common proinflammatory cytokines, in the mouse liver were



measured using ELISA kits purchased from ExCell Bio (Shanghai, China).

### Statistical analysis

The results are presented as the mean  $\pm$  standard deviation. Differences among the different treatments were evaluated by one-way analysis of variance (ANOVA) followed by a *post hoc* Tukey HSD test. The statistical difference is considered to be significant when  $p < 0.05$ . For the XPS analysis, the data obtained were analyzed with CasaXPS software. All the experimental data were processed with Origin 2021b (OriginLab Corp., USA).

## Results

### Adsorption of As(III) on CeO<sub>2</sub> NPs in sGIFs and pH adjusted UPW

As shown in Fig. 1, both 30 nm and 10 nm CeO<sub>2</sub> NPs strongly adsorbed As(III). In sGIFs and UPW, the  $q_t$  of 30

nm CeO<sub>2</sub> NPs generally increased along the digestive tract or as the incubation time increased. This trend was more obvious at higher spiked concentrations of As(III) (Fig. 1A and B, Table S4<sup>†</sup>). However, the  $q_t$  of 10 nm CeO<sub>2</sub> NPs exhibited a distinctive trend compared to that of 30 nm CeO<sub>2</sub> NPs. For instance, the  $q_t$  of As on 10 nm CeO<sub>2</sub> NPs kept decreasing along with the digestion process. In Lev 6, the  $q_t$  of 10 nm CeO<sub>2</sub> NPs dropped from saliva to gastric juice to intestinal juice as the digestion proceeded. For UPW, the  $q_t$  of 10 nm CeO<sub>2</sub> NPs did not change much at Lev 1, 2 and 3, but increased with the incubation time (along with the change in pH) at Lev 4, 5 and 6. (Fig. 1C and D, Table S5<sup>†</sup>).

Corresponding to the increased  $q_t$  of 30 nm CeO<sub>2</sub> NPs, the bioaccessibility of As(III) generally decreased as digestion continued (Fig. 2A, Table S6<sup>†</sup>) and the decreasing trend was even more obvious in the case of UPW (Fig. 2B, Table S6<sup>†</sup>). For 10 nm CeO<sub>2</sub> NPs, the As bioaccessibility generally increased as digestion proceeded (Fig. 2C, Table S7<sup>†</sup>). In the

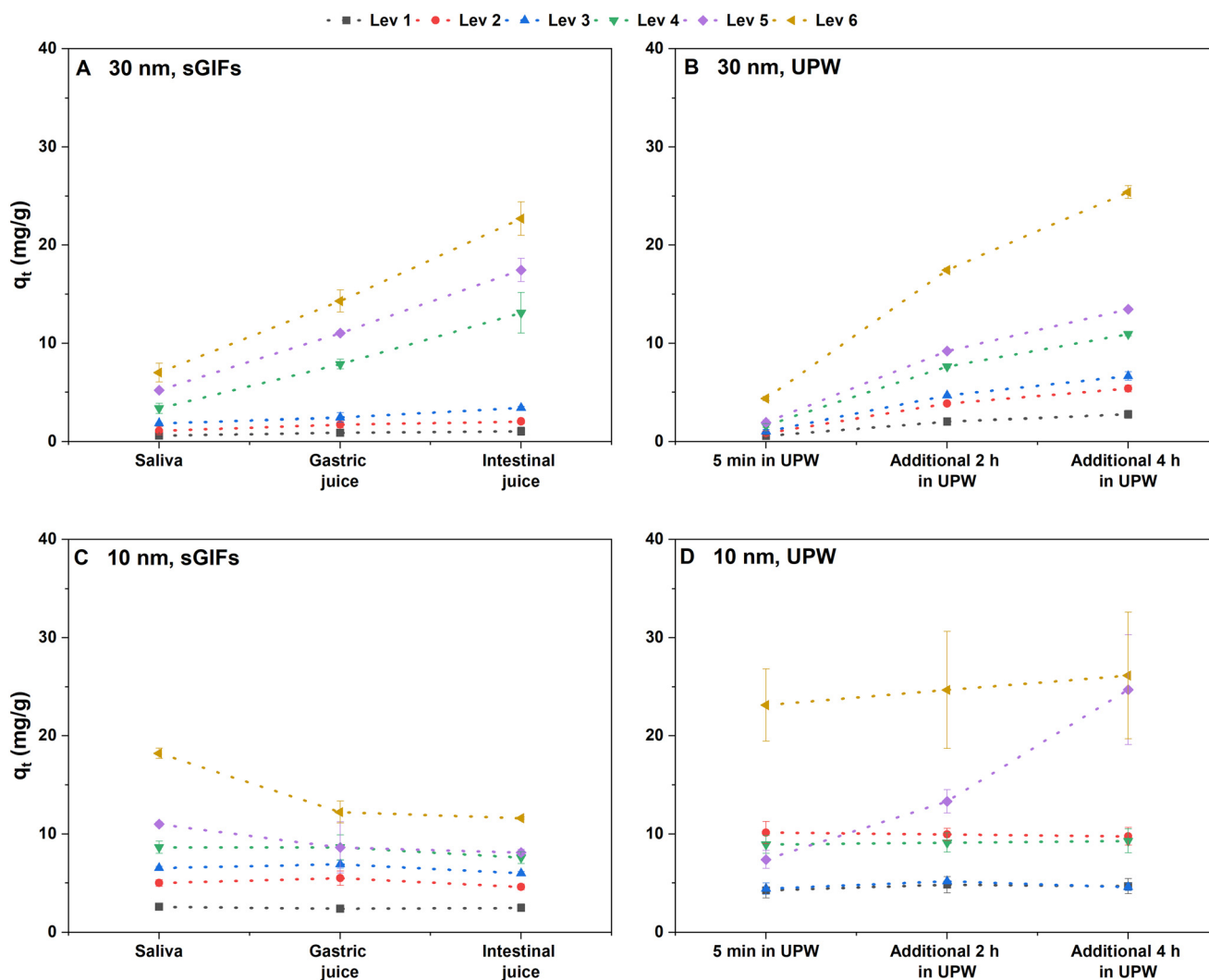


Fig. 1 The adsorption capacities of 30 nm CeO<sub>2</sub> NPs for As(III) in (A) sGIFs and (B) UPW. The adsorption capacities of 10 nm CeO<sub>2</sub> NPs for As(III) in (C) sGIFs and (D) UPW ( $n = 3$ ).



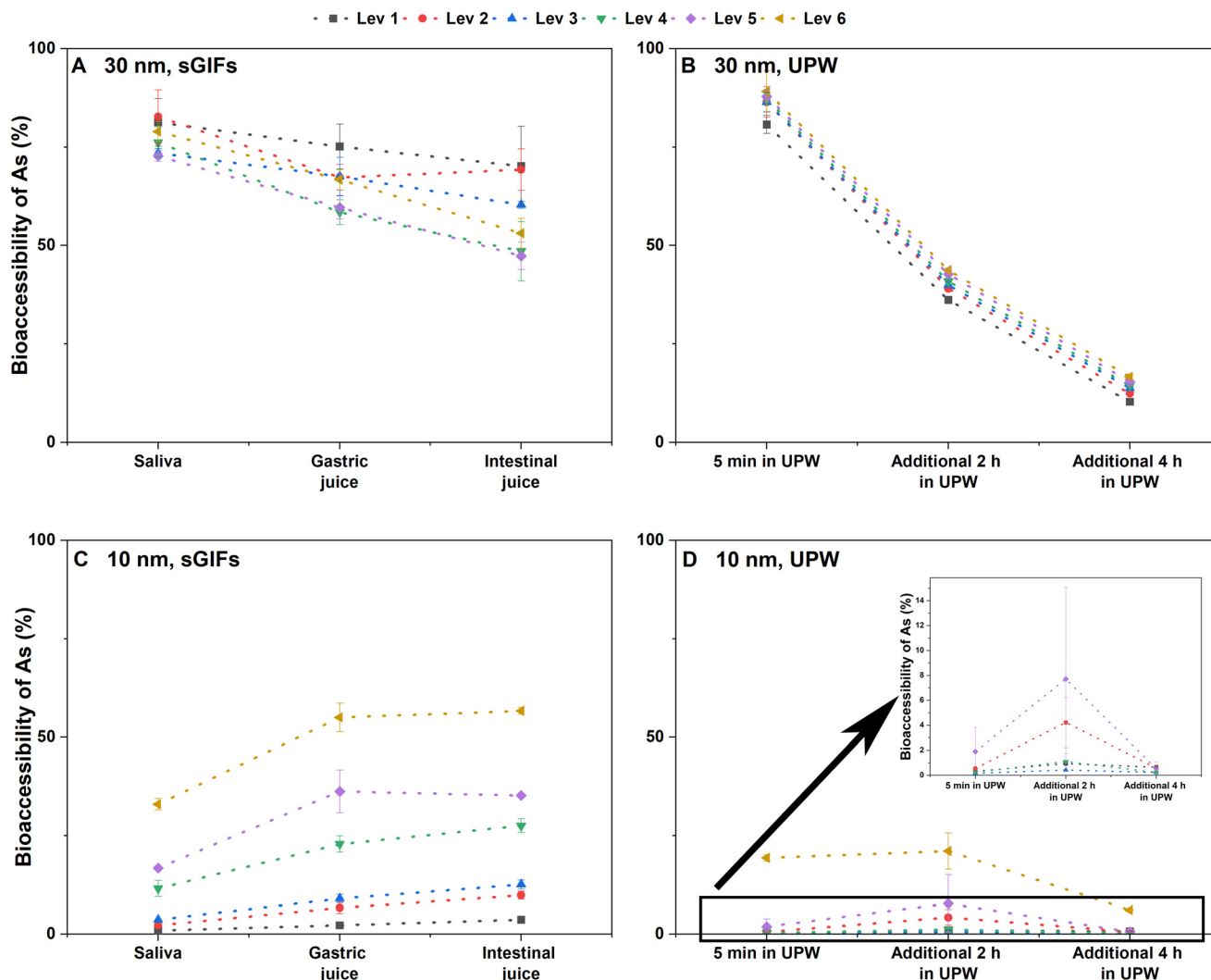


Fig. 2 Bioaccessibilities of As when it co-existed with  $\text{CeO}_2$  NPs in different matrices. (A) With 30 nm  $\text{CeO}_2$  NPs in sGIFs; (B) with 30 nm  $\text{CeO}_2$  NPs in UPW; (C) with 10 nm  $\text{CeO}_2$  NPs in sGIFs; (D) with 10 nm  $\text{CeO}_2$  NPs in UPW ( $n = 3$ ). An enlarged plot of Lev 1 to Lev 5 is shown as an inset figure in (D).

case of UPW, there was a decrease of As bioaccessibility at pH 7.5 (Fig. 2D, Table S7†).

### $\text{CeO}_2$ NPs and $\text{As(III)}$ interactions alter NP physicochemical properties

Based on the results of the adsorption experiment above, in the case of Lev 6, both the  $q_t$  of  $\text{CeO}_2$  NPs and bioaccessibility of As in sGIFs showed significant differences among the three phases of digestion. To decipher the interaction between  $\text{As(III)}$  and  $\text{CeO}_2$  NPs, the  $\text{CeO}_2$  NP physicochemical properties were characterized with different techniques, including DLS and XPS, and the comparison was carried out between Lev 0 and Lev 6 in sGIFs and UPW.

Table 1 summarizes the zeta potential and  $D_H$  of  $\text{CeO}_2$  NPs in sGIFs and in UPW. In sGIFs, the adsorption of  $\text{As(III)}$  barely changed the zeta potential of both 10 nm and 30 nm  $\text{CeO}_2$  NPs compared to the cases where  $\text{CeO}_2$  NPs

were suspended in sGIFs alone. Yet, the change in zeta potential at different sGIF phases or pH was greater in the case of 10 nm  $\text{CeO}_2$  NPs than in 30 nm  $\text{CeO}_2$  NPs. For 10 nm  $\text{CeO}_2$  NPs in UPW, there was a change in zeta potential from slightly positive to slightly negative upon the addition of  $\text{As(III)}$  at pH 6.4, but it had a minor impact on the zeta potential of 10 nm  $\text{CeO}_2$  NPs at other pH values. With regard to the  $D_H$ , the addition of  $\text{As(III)}$  significantly increased the  $D_H$  of 10 nm  $\text{CeO}_2$  NP aggregates in sGIFs; however, the size of the aggregates decreased in the case of UPW. With regard to 30 nm  $\text{CeO}_2$ , the hydrodynamic size decreased upon the addition of  $\text{As(III)}$  in both sGIFs and UPW.

XPS was used to investigate the oxidation states of Ce on the  $\text{CeO}_2$  NP surfaces, and the percentages of  $\text{Ce(III)}$  are summarized in Table 2. We monitored the oxidation states of As on the  $\text{CeO}_2$  NPs, but the amounts of As adsorbed on the surface were below the LOQ of XPS. Therefore, to explore the possible redox reactions between



**Table 1** Hydrodynamic diameter and zeta potential of CeO<sub>2</sub> NPs in UPW and sGIFs (*n* = 3). Lev 0 and Lev 6 refer to the cases where the initial concentrations of As(III) are 0 and 92 mg L<sup>-1</sup>, respectively

		Zeta potential (mV)		Hydrodynamic diameter (nm)	
		Lev 0	Lev 6	Lev 0	Lev 6
30 nm CeO <sub>2</sub> NPs	5 min in UPW (pH 6.4)	-75.70 ± 2.74	-63.21 ± 8.11	467 ± 18	365 ± 7
	Saliva	-32.53 ± 0.55	-31.63 ± 0.12	456 ± 19	418 ± 29
	Additional 2 h in UPW (pH 2)	-9.77 ± 3.19	-14.50 ± 3.20	2151 ± 137	1145 ± 93
	Gastric juice	-9.96 ± 0.34	-8.51 ± 0.73	605 ± 21	571 ± 34
	Additional 4 h in UPW (pH 7.5)	-58.80 ± 0.16	-62.38 ± 1.47	849 ± 33	530 ± 27
10 nm CeO <sub>2</sub> NPs	Intestinal juice	-22.45 ± 1.29	-21.62 ± 1.27	483 ± 27	482 ± 7
	5 min in UPW (pH 6.4)	4.65 ± 2.73	-4.80 ± 2.70	4765 ± 105	2582 ± 148
	Saliva	-27.04 ± 0.92	-26.70 ± 2.88	3590 ± 349	3825 ± 225
	Additional 2 h in UPW (pH 2)	46.70 ± 0.11	54.70 ± 0.10	3525 ± 104	2736 ± 21
	Gastric juice	-12.22 ± 0.38	-10.67 ± 0.58	3071 ± 96	3190 ± 419
	Additional 4 h in UPW (pH 7.5)	-55.37 ± 0.05	-58.90 ± 2.12	3443 ± 290	2215 ± 100
	Intestinal juice	-18.88 ± 2.66	-17.77 ± 2.22	3303 ± 133	5529 ± 53

CeO<sub>2</sub> NPs and As(III), we compared the oxidation states of Ce on the NP surface with and without As. A clear difference was observed (Table 2) when As(III) was adsorbed onto both 10 nm and 30 nm CeO<sub>2</sub> NPs compared with the CeO<sub>2</sub> NPs suspended in sGIFs, *i.e.* the percentage of Ce(III) on the CeO<sub>2</sub> NP surface increased after the adsorption of As(III).

#### Altered biodistribution of tAs and Ce by co-exposure

The concentrations of Ce in the mouse liver, kidney and spleen in mice after oral exposure to CeO<sub>2</sub> NPs and/or As(III) are shown in Fig. 3, and the relative bioavailabilities of Ce are shown in Table 3. CeO<sub>2</sub> NPs were found to be mainly deposited in these three organs, while the concentrations of Ce in other tested organs were below the LOQ of ICP-MS (data not shown). When mice were co-exposed to 30 nm CeO<sub>2</sub> NPs and As(III), the accumulation of Ce in the liver was significantly increased (+40%) (Fig. 3) and the relative bioavailability of Ce was also increased to 4.19 ± 0.29% (*p* < 0.05) (Table 3) compared to the case where mice were exposed to NPs alone. In mice co-exposed to 10 nm CeO<sub>2</sub> NPs and As(III), the presence of As(III) only slightly decreased the accumulation of Ce in the liver (by 10%) and kidney (by 16%) (Fig. 3).

Compared to the deposition of CeO<sub>2</sub> NPs, tAs was found to be distributed widely in the tested organs, including the mouse liver, bladder, brain, kidney, and spleen, as shown in

**Table 2** Percentage of Ce(III) on the CeO<sub>2</sub> NP surface. Lev 0 and Lev 6 refer to the cases where the initial concentrations of As(III) are 0 and 92 mg L<sup>-1</sup> respectively

		Ce(III)	
		Lev 0	Lev 6
30 nm CeO <sub>2</sub> NPs	Saliva	53.8%	55.6%
	Gastric juice	56.9%	63.2%
	Intestinal juice	58.4%	62.3%
10 nm CeO <sub>2</sub> NPs	Saliva	52.6%	54.4%
	Gastric juice	57.4%	67.3%
	Intestinal juice	59.6%	61.2%

Fig. 4A–E. Compared with the mice exposed to As(III) alone, the levels of tAs in the liver, bladder, kidney and spleen were significantly lower (decreases of 44%, 37%, 43% and 47%, respectively) in the group co-exposed to 10 nm CeO<sub>2</sub> NPs and As(III). Moreover, 30 nm CeO<sub>2</sub> NPs significantly increased the relative bioaccessibility of As to 2.93 ± 0.20% (*p* < 0.05) (Table 3). With regard to mice co-exposed to 10 nm CeO<sub>2</sub> NPs and As(III), the accumulation of As in the mouse liver and kidney was significantly decreased (Fig. 4A and D), and the As relative bioavailability showed a 38% decrease compared with the individual oral exposure to As(III) (Table 3), indicating that 10 nm CeO<sub>2</sub> NPs significantly decreased the *in vivo* uptake of As.

#### Altered metabolism of As(III) by co-exposure with CeO<sub>2</sub> NPs

It is well accepted that the toxicity of As is related to both its concentration and chemical form, where inorganic forms (*e.g.* As(III) and As(V)) are more toxic than the methylated forms (*e.g.* MMA and DMA).<sup>33</sup> Therefore, the sole determination of total As (tAs) is not enough for the investigation of As toxicity,<sup>34</sup> and it is necessary, also, to determine the As species in mice tissues. The metabolism, mainly referring to reduction and biomethylation of As, mainly happens in the liver.<sup>35</sup> Therefore, the speciation of As was investigated using the liver tissues.

Fig. S5† shows the LC-ICP-MS elution profiles of As(III) (6.9 min), DMA (8.4 min), MMA (14.8 min) and As(V) (21.0 min) species in the liver. The four known As species were identified with some unknown species (uAs). It is expected that arsenic can react with proteins readily and other As-containing metabolites may form after the exposure. The concentrations of As species (As(III), As(V), MMA, DMA and uAs) in the liver are presented in Fig. 5A, and the percentages of each As species are shown in Fig. 5B. The major components of As species in the liver of mice exposed to the 30 nm CeO<sub>2</sub> NP–As(III) mixture were As(III) and DMA (5.15 ± 0.8 ng g<sup>-1</sup> and 1.74 ± 0.36 ng g<sup>-1</sup>, respectively; accounting for 9.9% and 3.3% of tAs, respectively). In the case of the co-exposure to 10 nm CeO<sub>2</sub>







Fig. 3 The concentrations of Ce in the (A) liver, (B) kidney and (C) spleen of mice ( $n = 4$ ). The symbols “a” and “b” represent significant difference ( $p < 0.05$ ) between the control group and corresponding individual NP exposure group, respectively.

NPs and As(III), the major As species were As(III) and As(V) ( $2.51 \pm 0.80 \text{ ng g}^{-1}$  and  $1.70 \pm 1.40 \text{ ng g}^{-1}$ , respectively, accounting for 8.3% and 5.6% of tAs). For the mice exposed to As(III) alone, the major As metabolites in the liver were As(III) and As(V) ( $3.13 \pm 1.12 \text{ ng g}^{-1}$  and  $0.75 \pm 0.27 \text{ ng g}^{-1}$ , respectively, accounting for 5.7% and 1.4% of tAs, respectively). To summarize, the As metabolites in the liver were similar in the groups exposed to As(III) alone and co-exposed to 10 nm CeO<sub>2</sub> NPs and As(III), but the presence of 30 nm CeO<sub>2</sub> NPs altered the As metabolism.

#### Toxicological assessment of co-exposure to CeO<sub>2</sub> NPs and As(III)

Fig. S4A† shows the changes in the mouse body weight during the animal study, and Fig. S4B–F† present the relative weights (organ weight/body weight) of the tested organs. All mice under different experimental conditions had no obvious loss of body weight during the entire experimental period. However, a noticeable decrease in the relative weight of the liver (liver weight/body weight) was observed in mice exposed to As(III) alone as well as the 30 nm CeO<sub>2</sub> NP–As(III) mixture. This indicates that both exposure to As alone and co-exposure to 30 nm CeO<sub>2</sub> NPs and As(III) had a certain impact on the liver. The ALT activity level in serum increased significantly in these two experimental groups, providing further evidence that these two treatments damaged the liver (Fig. 6A). Worse still, the LDH activity level in serum in mice co-exposed to 30 nm CeO<sub>2</sub> NPs and As(III) was significantly

higher than that in mice exposed to As(III) alone, and the level in mice treated with 30 nm CeO<sub>2</sub> NPs and As(III) was 1.3-fold higher than that in mice exposed to As(III) alone (Fig. 6B). This suggests combined toxicity in the mice co-exposed to 30 nm CeO<sub>2</sub> NPs and As(III). Although co-exposure to 10 nm CeO<sub>2</sub> NPs and As(III) increased the creatine and LDH levels in serum compared with those in the control mice, the creatine and LDH levels were significantly lower than those in mice exposed to As(III) alone (Fig. 6A and B). Co-exposure to 10 nm CeO<sub>2</sub> NPs and As(III) did not significantly increase the ALT level in serum (Fig. 6C). This indicates that the 10 nm CeO<sub>2</sub> NPs alleviate the toxicity of As(III) in mice. The ROS level and inflammatory response were examined in the liver, with results shown in Fig. 7. A significant decrease in the activity of SOD was observed in mice treated with As(III) alone and the 30 nm CeO<sub>2</sub> NP–As(III) mixture compared with the control group (Fig. 7A). This suggests that the decreased activity of this antioxidant enzyme increased the oxidative stress in the liver. The concentrations of TNF- $\alpha$  and IL-1 $\beta$  were increased in groups exposed to 30 nm CeO<sub>2</sub> NPs or As(III) alone and the 30 nm CeO<sub>2</sub> NP–As(III) mixture (Fig. 7B and C). Co-exposure to 30 nm CeO<sub>2</sub> NPs and As(III) significantly increased the levels of these two pro-inflammatory cytokines in the liver compared with the individual exposure to As(III) or 30 nm CeO<sub>2</sub> NPs. Vacuolar degeneration observed in the liver further confirmed that oral exposure to As(III) and co-exposure to 30 nm CeO<sub>2</sub> NPs and As(III) induced liver injury (Fig. 8).

Table 3 The relative bioavailability of Ce and As in mice, which was determined using the sum concentrations of Ce in the mouse liver, spleen and kidney, or the sum concentrations of As in the mouse liver, bladder, brain, kidney and spleen ( $n = 4$ )

	Relative bioavailability of Ce (‰)	Relative bioavailability of As (%)
Control	—	—
30 nm	$3.65 \pm 0.28$	—
30 nm + As	$4.19 \pm 0.29^a$	$2.93 \pm 0.20^b$
10 nm	$2.26 \pm 0.30$	—
10 nm + As	$2.06 \pm 0.32$	$1.53 \pm 0.17^b$
As	—	$2.48 \pm 0.25$

<sup>a</sup> Compared with the individual exposure to 30 nm CeO<sub>2</sub> NPs ( $p < 0.05$ ). <sup>b</sup> Compared with the individual exposure to As(III) ( $p < 0.05$ ).



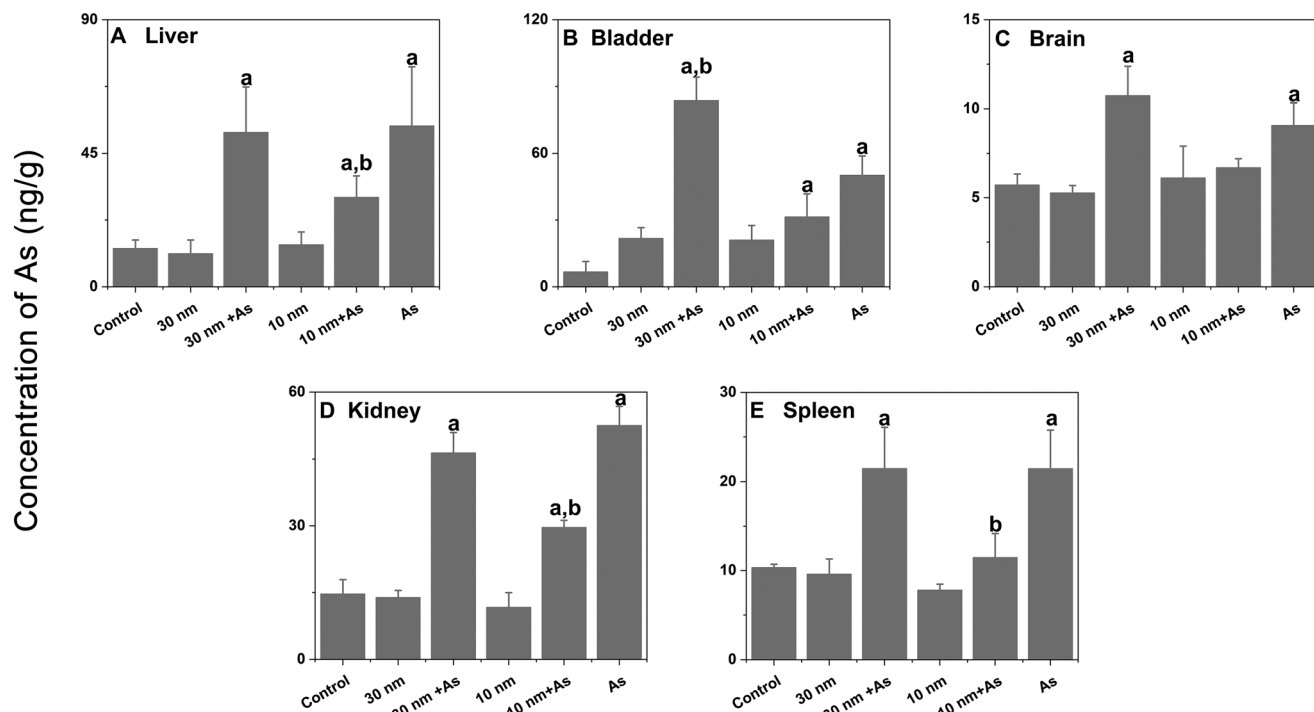


Fig. 4 The concentrations of tAs in the (A) liver, (B) bladder, (C) brain, (D) kidney and (E) spleen of mice ( $n = 4$ ). The symbols “a” and “b” represent significant difference ( $p < 0.05$ ) between the control group and As(III) alone exposure group, respectively.

## Discussion

### Behaviors of CeO<sub>2</sub> NPs and As(III) in sGIFs and at different pH values

The presence of sGIFs and pH value changes may have an influence on the adsorption capacity ( $q_t$ ) and physicochemical properties (hydrodynamic size or zeta potential) of the NPs. Since there was lack of information about the coating of the CeO<sub>2</sub> NPs used, and the As(III) concentrations in each step were not the same, no direct

comparison will be made between the two CeO<sub>2</sub> NPs in this work. As the concentrations of CeO<sub>2</sub> NPs and As(III) available for adsorption were changing in each step after sampling, the behavior or fate of the components in every step was considered separately but not as a continuous process.

sGIFs can have different effects on the adsorption of As(III) in different CeO<sub>2</sub> NPs. For 30 nm CeO<sub>2</sub> NPs, there was no obvious difference in the adsorption of As(III) in sGIFs and UPW. In general, the  $q_t$  of 30 nm CeO<sub>2</sub> NPs

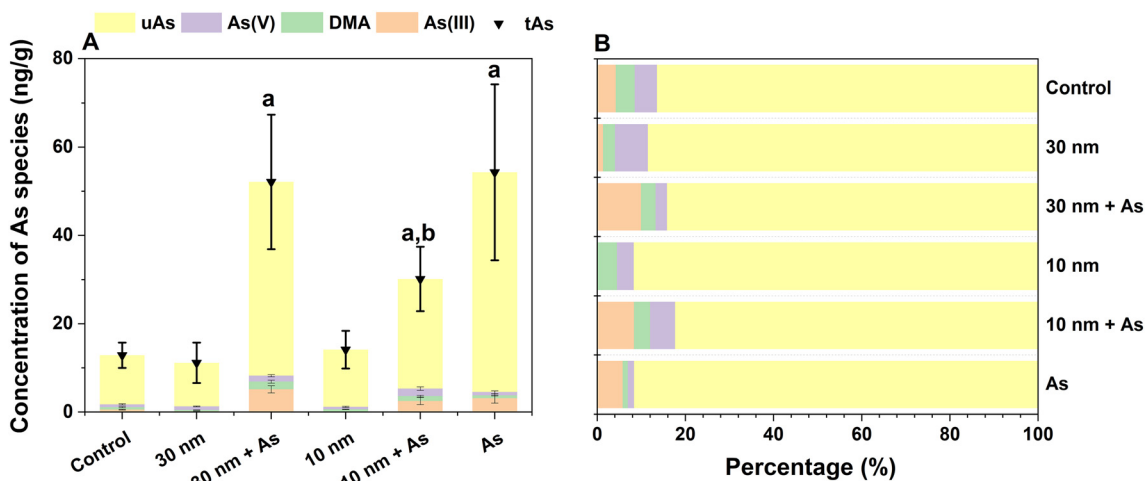


Fig. 5 The concentrations of total As (tAs) and As species in the mouse liver (A) ( $n = 4$ ). The portion of each As species in the mouse liver (B) ( $n = 4$ ). The symbols “a” and “b” represent significant difference ( $p < 0.05$ ) between the control group and As(III) alone exposure group, respectively.



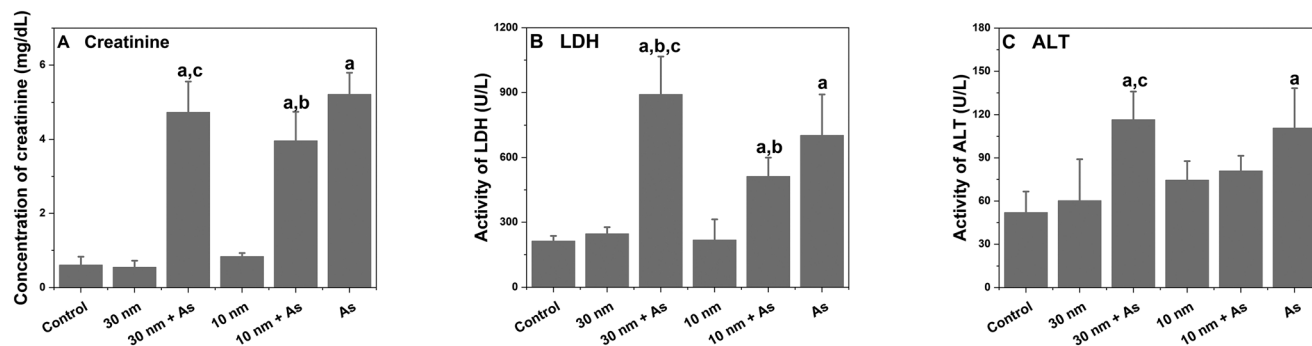


Fig. 6 The concentrations of creatinine (A) and activities of LDH (B) and ALT (C) in serum ( $n = 4$ ). The symbols “a”, “b” and “c” represent significant difference ( $p < 0.05$ ) between the control group, As(III) alone exposure group and corresponding individual NP exposure group, respectively.

showed an increasing trend as the digestion proceeded, resulting in the decreased bioaccessibility of As in the sGIFs, with a similar observation obtained in UPW (Fig. 1). While NP  $D_H$  values increased in sGIFs by 31–74%, they were below 650 nm (Table 1). Within this range, a higher colloidal stability was observed, and the CeO<sub>2</sub> NPs were well-dispersed in the aqueous solution.<sup>29</sup> It is proposed that the strong repulsive forces derived from the highly negative zeta potential of 30 nm CeO<sub>2</sub> NPs accounted for the minor changes in  $D_H$  of NPs in the saliva and intestinal juice. Although the zeta potential of the NPs became less negative in the gastric juice due to the low pH in the stomach, the  $D_H$  was not altered much by the NPs adsorbed with As(III) (Table 1). This might be because the corona formed around NPs acted as a colloidal stabilizer during the digestive process.<sup>36</sup> The slight aggregation reflected by the minor alteration in the hydrodynamic size suggests that the adsorption of As(III) continued along the GIT. With the increased  $q_t$  of 30 nm CeO<sub>2</sub> NPs for As(III), the bioaccessibility of As in the GIT decreased from the mouth to the intestine (Fig. 2A). The absence of a matrix in UPW resulted in a similar but more apparent trend in the behavior of CeO<sub>2</sub> NPs and bioaccessibility of As(III). The aggregation status and

charge of CeO<sub>2</sub> NPs also presented a similar change to that in the GIT.

10 nm CeO<sub>2</sub> NPs were more prone to aggregation in sGIFs, as indicated by increasing  $D_H$  of 10 nm CeO<sub>2</sub> NPs over 3000 nm in sGIFs. (Table 1). Neil *et al.*<sup>29</sup> observed that CeO<sub>2</sub> NPs with over 2000 nm  $D_H$  settled quickly from the solution after 4 h. The aggregation of 10 nm CeO<sub>2</sub> NPs decreased the number of adsorption sites of As(III). With the extensive aggregation, the accessible adsorption sites of 10 nm CeO<sub>2</sub> NPs decreased, reducing the  $q_t$  of NPs along the GIT, leading to an increased bioaccessibility of As along different phases in sGIFs (Fig. 2C). Again, the corona formation in the sGIFs can be accounted for the small fluctuation in As(III) adsorption or hydrodynamic size of NPs, regardless of the change in zeta potential.

The behavior of 10 nm CeO<sub>2</sub> NPs in UPW did not show a similar trend to that in the sGIFs. It can be seen that, even though the  $q_t$  of As(III) remained at a similar level at different pH values, there is no direct relationship of its adsorption power with the hydrodynamic size, as well as the As bioaccessibility. It is difficult to fully explain this behavior because there may exist other modes of interaction between the 10 nm CeO<sub>2</sub> NPs and As(III) apart from electrostatic interaction.

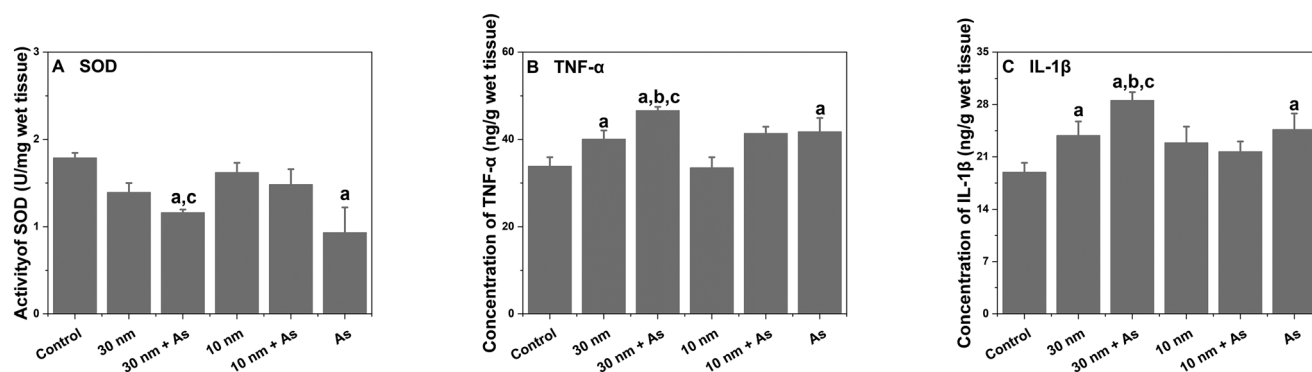


Fig. 7 Activity of SOD (A), as an evaluation of oxidative stress, was measured in the liver. The inflammation level in the liver was confirmed by the concentrations of TNF- $\alpha$  (B) and IL-1 $\beta$  (C) ( $n = 4$ ). The symbols “a”, “b” and “c” represent significant difference ( $p < 0.05$ ) between the control group, As(III) alone exposure group and corresponding individual NP exposure group, respectively.



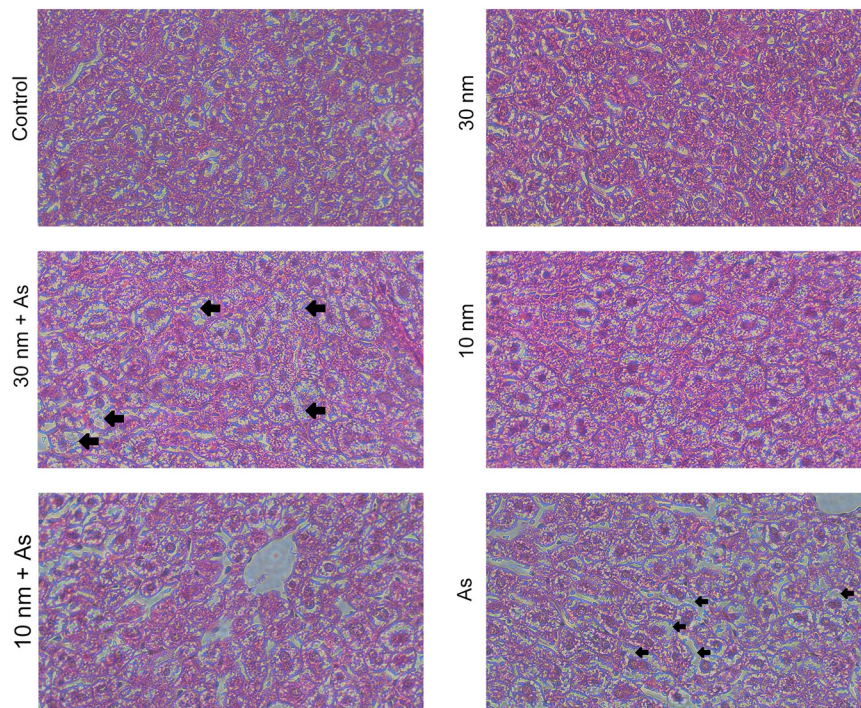


Fig. 8 Histopathological examination of the mouse liver after treatment. Vacuolar degenerations are indicated with arrows (magnification = 50 $\times$ ).

### Biological fate and joint effects of CeO<sub>2</sub> NPs and As(III) in mice

To evaluate the impact of CeO<sub>2</sub> NP and As(III) co-exposure on their biological fate in mice, the mice were co-exposed to CeO<sub>2</sub> NPs and As(III) with dosages similar to the concentration levels of CeO<sub>2</sub> NPs and As(III) at Lev 6 in the *in vitro* GIT model. In this way, the information of CeO<sub>2</sub> NP adsorption capacity, as bioaccessibility, and the physicochemical properties of CeO<sub>2</sub> NPs ascertained in the *in vitro* GIT model could be used to help study the behavior of CeO<sub>2</sub> NPs and As(III) *in vivo*. The  $q_t$  of CeO<sub>2</sub> NPs and the bioaccessibility of As mentioned in the following discussion refer to the case of Lev 6 in the *in vitro* GIT model.

Adsorption of metal(loid)/metal ions onto NPs changes their surface charge and their dynamic behavior in solution, altering their biological fate (*e.g.* bioaccumulation, metabolism and excretion) in organisms.<sup>17,18,37</sup> In this animal study, CeO<sub>2</sub> NPs and As(III) had mutual effects on their *in vivo* biological fates. Surprisingly, we found that the bioaccumulation/bioavailability of As was not identical to the results of As bioaccessibility obtained through the *in vitro* GIT model in the case of 30 nm CeO<sub>2</sub> NPs.

When mice were orally exposed to the 30 nm CeO<sub>2</sub> NP-As(III) mixture, the accumulation of Ce increased in the liver compared to the individual 30 nm CeO<sub>2</sub> NP exposure, while the accumulation of tAs in the liver was comparable with the individual As(III) exposure. In sGIFs, the adsorption of As(III) onto CeO<sub>2</sub> NPs slightly increased the zeta potential and decreased the  $D_H$  of the NPs. This may account for the increased uptake of CeO<sub>2</sub> NPs because NPs with small size

and less negative charge pass through the small intestine's mucus layer more easily.<sup>38</sup> Although the 30 nm CeO<sub>2</sub> NPs decreased the bioaccessibility of As to 53% in simulated intestinal juice, the increased uptake of 30 nm CeO<sub>2</sub> NPs adsorbed with As(III) actually increased the bioavailability of As in the liver, resulting in the relatively higher As bioaccumulation in the liver. Furthermore, the co-exposure significantly increased the relative bioaccessibility of Ce and As in mice, suggesting that co-exposure to 30 nm CeO<sub>2</sub> NPs and As(III) increased the uptake of both contaminants (Table 3). In the case of 10 nm CeO<sub>2</sub> NPs, the adsorption of As(III) onto NPs significantly decreased the bioaccessibility of As to 57% in intestinal juice, resulting in less accumulation of tAs in the mouse liver, brain, kidney and spleen compared to the individual exposure to As(III). Moreover, the aggregation of NPs in the GIT ( $D_H > 2000$  nm) strongly inhibited the uptake of NPs, leading to the low deposition level of Ce in the organs. Although Ce was observed to be deposited in the liver and spleen, the decreased  $q_t$  of 10 nm CeO<sub>2</sub> NPs in intestinal juice and the relatively low uptake of 10 nm CeO<sub>2</sub> NPs limited the amount of As(III) that accumulated in the liver. In other words, co-exposure with 10 nm CeO<sub>2</sub> NPs decreased the bioaccessibility, relative bioavailability and bioaccumulation of As in mice. Our study suggested that, in the co-exposure study of NPs and metal(loid) ions, the assessment of metal(loid) ion bioaccessibility using the *in vitro* GIT model neglected the possibility that NPs adsorbed with metal(loid) ions could act as "Trojan horses" and deliver metal(loid) ions into organs. This would explain the inconsistent results between the bioaccessibility assessment and bioavailability/



bioaccumulation assessment. The physicochemical properties of NPs in sGIFs, especially their zeta potential and  $D_H$ , provide supplementary information to evaluate the possible “Trojan horse” effect of NPs.

CeO<sub>2</sub> NPs influenced not only the bioaccumulation/bioaccessibility of As in mice, but also the As metabolism in the liver. In the *in vitro* GIT model, the Ce(III) content on the NP surface increased when As(III) was adsorbed onto the NPs in the three phases of sGIFs (Table 2). The change of Ce(III) content indicated that, in sGIFs, redox interactions of Ce(IV) and As(III) took place on the surface of CeO<sub>2</sub> NPs compared to CeO<sub>2</sub> NPs alone. Neil *et al.*<sup>29</sup> and Bi *et al.*<sup>28</sup> also observed this phenomenon when As(III) was adsorbed onto CeO<sub>2</sub> NPs in water. Corresponding to the redox reaction observed in the *in vitro* GIT model, the percentage of As(V) in the CeO<sub>2</sub> NP (both 10 nm and 30 nm) and As(III) co-exposure group was larger than that in mice exposed to As(III) alone. Moreover, the percentages of As(III) and DMA also increased in the co-exposure group compared to the group exposed to As(III) alone, indicating that CeO<sub>2</sub> NPs restrained the metabolism of As in the liver. The mechanism of this phenomenon deserves further investigation.

The combined toxicity of CeO<sub>2</sub> NPs and As(III) has been investigated using *in vitro* models in previous studies: CeO<sub>2</sub> NPs were found to reduce the toxicity of As(III) to human bronchial epithelial cells as well as to A549 human cells as a result of the effective reduction of available As(III) through adsorption.<sup>39,40</sup> However, the combined toxicity of CeO<sub>2</sub> NPs and As(III) has never been investigated using an *in vivo* model. Moreover, in previous studies where combined toxicity of NPs and toxic elements by oral exposure was investigated using mice as an *in vivo* model,<sup>17,18,41</sup> the lack of confirmation and characterization of NPs adsorbed with toxic elements in the GIT leads to insufficient understanding of the underlying mechanism of joint toxicity. To our knowledge, this is the first study to investigate the joint effects of CeO<sub>2</sub> NPs and As(III) after their oral co-exposure in mice based on an *in vitro* GIT model as well as an *in vivo* study in mice. Our results suggest that the joint toxicity of CeO<sub>2</sub> NPs and As(III) results from altered Ce and As bioaccumulation in organs and from the redox reaction between As(III) and Ce(IV) on NP surfaces after adsorption.

When mice were co-exposed to 10 nm CeO<sub>2</sub> NPs and As(III), the adsorption of As(III) on the NP surface promoted the aggregation of NPs, preventing the intestinal uptake of NPs with adsorbed As. Moreover, the adsorption of As onto NPs along the GIT decreased both the bioaccessibility and the bioavailability of As. As a result, an antagonistic effect was observed in the exposure to the 10 nm CeO<sub>2</sub> NP-As(III) mixture. However, in the case of exposure to the 30 nm CeO<sub>2</sub> NP-As(III) mixture, the adsorption of As(III) onto NPs increased the accumulation of CeO<sub>2</sub> NPs in the liver and resulted in a relatively higher level of tAs deposited in organs. In other words, 30 nm CeO<sub>2</sub> NPs adsorbed with As(III) had a “Trojan horse” effect in delivering As to cells. The adsorption of As(III) on CeO<sub>2</sub>

NPs decreased the redox activity of NPs,<sup>28</sup> and the enhanced portion of Ce(III) on the NP surface as a result of the redox reaction between As(III) and Ce(IV) made the NPs more toxic.<sup>42,43</sup> The results showed that CeO<sub>2</sub> NPs also altered the As metabolism in the liver, and this may have contributed to the combined toxicity observed in mice co-exposed to 30 nm CeO<sub>2</sub> NPs and As(III).

## Conclusion

Our study demonstrated that CeO<sub>2</sub> NPs exhibit strong adsorption capacity towards As(III), even during simulated digestion. The strong adsorption of As(III) onto CeO<sub>2</sub> NPs is expected to impact their biological fate, depending on the alterations of NP physicochemical properties. In the case of 30 nm CeO<sub>2</sub> NPs and As(III), due to the NPs' hydrodynamic diameter as well as the zeta potential of NPs, which facilitated the intestinal uptake of NPs in sGIFs, the co-exposure resulted in the enhanced Ce and As relative bioavailability in mice. Furthermore, the redox reaction between As(III) and Ce(IV) increased the toxicity of NPs, and CeO<sub>2</sub> NPs affected the As metabolism in the liver. Collectively, combined toxicity was observed. The adsorption of As(III) onto 10 nm CeO<sub>2</sub> NPs promoted the aggregation of NPs in the GIT, preventing the intestinal uptake of both NPs and As(III). Therefore, oral co-exposure to 10 nm CeO<sub>2</sub> NPs and As(III) showed mitigating effects on toxicity in mice.

To the best of our knowledge, this is the first study to explore the biological fate of CeO<sub>2</sub> NPs and As(III) in mice after their oral co-exposure by linking the behavior of the particles during the digestive process and their bioaccumulation/toxicity. The complementary information provided by the *in vitro* GIT model and *in vivo* mouse model enables us to have a better understanding of the joint effects of NPs and other contaminants on mice. The findings of this study demonstrated that the adsorption of contaminants onto NPs changed the NP physicochemical properties in the GIFs, and thus changed the NP biological fate, including their bioaccumulation as well as their toxicity in mice.

## Author contributions

Huang Yingyan: conceptualization, methodology, investigation, writing – original draft. Judy Tsz-Shan Lum: conceptualization, methodology, writing – review & editing. Wai-Kit Ho: writing – review & editing. Kelvin Sze-Yin Leung: writing – review & editing, supervision.

## Conflicts of interest

There are no conflicts to declare.

## Acknowledgements

Kelvin Sze-Yin Leung thanks the funding support from the Hong Kong Research Grants Council (HKBU 12303122 and 12302821). Y. Huang is supported by a postgraduate



studentship offered by the University Grants Committee. Authors also extend acknowledgement to <https://BioRender.com> for creation of images.

## References

- N. Prajitha, S. S. Athira and P. V. Mohanan, Bio-interactions and risks of engineered nanoparticles, *Environ. Res.*, 2019, **172**, 98–108.
- B. Nowack and T. D. Bucheli, Occurrence, behavior and effects of nanoparticles in the environment, *Environ. Pollut.*, 2007, **150**, 5–22.
- F. Tou, J. Wu, J. Fu, Z. Niu, M. Liu and Y. Yang, Titanium and zinc-containing nanoparticles in estuarine sediments: Occurrence and their environmental implications, *Sci. Total Environ.*, 2021, **754**, 142388.
- Y. Zheng, X. Chen, N. D. Joseph, Y. Zhang, H. Chen and B. Gao, in *Emerging Contaminants in Soil and Groundwater Systems*, ed. B. Gao, Elsevier, pp. 165–204.
- V. Srivastava, D. Gusain and Y. C. Sharma, Critical review on the toxicity of some widely used engineered nanoparticles, *Ind. Eng. Chem. Res.*, 2015, **54**, 6209–6233.
- J.-M. Exbrayat, E. N. Moudilou and E. Lapiéd, Harmful effects of nanoparticles on animals, *J. Nanotechnol.*, 2015, 861092.
- K. R. B. Singh, V. Nayak, T. Sarkar and R. P. Singh, Cerium oxide nanoparticles: properties, biosynthesis and biomedical application, *RSC Adv.*, 2020, **10**, 27194–27214.
- R. J. B. Peters, G. van Bommel, N. B. L. Milani, G. C. T. den Hertog, A. K. Undas, M. van der Lee and H. Bouwmeester, Detection of nanoparticles in Dutch surface waters, *Sci. Total Environ.*, 2018, **621**, 210–218.
- K. Phalyvong, Y. Sivry, H. Pauwels, A. Gélabert, M. Tharaud, G. Wille, X. Bourrat and M. F. Benedetti, Occurrence and origins of cerium dioxide and titanium dioxide nanoparticles in the Loire River (France) by single particle ICP-MS and FEG-SEM imaging, *Front. Environ. Sci.*, 2020, **8**, 141.
- K. Phalyvong, Y. Sivry, H. Pauwels, A. Gélabert, M. Tharaud, G. Wille, X. Bourrat, J. F. Ranville and M. F. Benedetti, Assessing CeO<sub>2</sub> and TiO<sub>2</sub> nanoparticle concentrations in the Seine River and its tributaries near Paris, *Front. Environ. Sci.*, 2021, **8**, 549896.
- L. N. Rand, K. Flores, N. Sharma, J. Gardea-Torresdey and P. Westerhoff, Quantifying nanoparticle associated Ti, Ce, Au, and Pd occurrence in 35 U.S. surface waters, *ACS ES&T Water*, 2021, **1**, 2242–2250.
- J. Sanchís, J. Jiménez-Lamana, E. Abad, J. Szpunar and M. Farré, Occurrence of cerium-, titanium-, and silver-bearing nanoparticles in the Besòs and Ebro rivers, *Environ. Sci. Technol.*, 2020, **54**, 3969–3978.
- R. Kaegi, A. Gogos, A. Voegelin, S. J. Hug, L. H. E. Winkel, A. M. Buser and M. Berg, Quantification of individual rare earth elements from industrial sources in sewage sludge, *Water Res.: X*, 2021, **11**, 100092.
- G. Cornelis, B. Ryan, M. J. McLaughlin, J. K. Kirby, D. Beak and D. Chittleborough, Solubility and batch retention of CeO<sub>2</sub> nanoparticles in soils, *Environ. Sci. Technol.*, 2011, **45**, 2777–2782.
- O.F.E.C.-O.A.D. (OECD), List of manufactured nanomaterials and list of endpoints for phase one of the OECD testing programme, 2008.
- I. Escher Beate, M. Stapleton Heather and L. Schymanski Emma, Tracking complex mixtures of chemicals in our changing environment, *Sci. Total Environ.*, 2020, **367**, 388–392.
- J. Jia, F. Li, S. Zhai, H. Zhou, S. Liu, G. Jiang and B. Yan, Susceptibility of overweight mice to liver injury as a result of the ZnO nanoparticle-enhanced liver deposition of Pb<sup>2+</sup>, *Environ. Sci. Technol.*, 2017, **51**, 1775–1784.
- C. Teng, J. Jia, Z. Wang and B. Yan, Oral co-exposures to zinc oxide nanoparticles and CdCl<sub>2</sub> induced maternal-fetal pollutant transfer and embryotoxicity by damaging placental barriers, *Ecotoxicol. Environ. Saf.*, 2020, **189**, 109956.
- M. Guo, X. Xu, X. Yan, S. Wang, S. Gao and S. Zhu, *In vivo* biodistribution and synergistic toxicity of silica nanoparticles and cadmium chloride in mice, *J. Hazard. Mater.*, 2013, **260**, 780–788.
- A. R. Donovan, C. D. Adams, Y. Ma, C. Stephan, T. Eichholz and H. Shi, Detection of zinc oxide and cerium dioxide nanoparticles during drinking water treatment by rapid single particle ICP-MS methods, *Anal. Bioanal. Chem.*, 2016, **408**, 5137–5145.
- S. Chowdhury, M. A. J. Mazumder, O. Al-Attas and T. Husain, Heavy metals in drinking water: Occurrences, implications, and future needs in developing countries, *Sci. Total Environ.*, 2016, **569–570**, 476–488.
- M. Troester, H. J. Brauch and T. Hofmann, Vulnerability of drinking water supplies to engineered nanoparticles, *Water Res.*, 2016, **96**, 255–279.
- K. Tiede, S. F. Hanssen, P. Westerhoff, G. J. Fern, S. M. Hankin, R. J. Aitken, Q. Chaudhry and A. B. A. Boxall, How important is drinking water exposure for the risks of engineered nanoparticles to consumers?, *Nanotoxicology*, 2016, **10**, 102–110.
- L. Voss, P. E. J. Saloga, V. Stock, L. Böhmert, A. Braeuning, A. F. Thünemann, A. Lampen and H. Sieg, Environmental impact of ZnO nanoparticles evaluated by *in vitro* simulated digestion, *ACS Appl. Nano Mater.*, 2019, **3**, 724–733.
- H. Sieg, C. Kastner, B. Krause, T. Meyer, A. Burel, L. Böhmert, D. Lichtenstein, H. Jungnickel, J. Tentschert, P. Laux, A. Braeuning, I. Estrela-Lopis, F. Gauffre, V. Fessard, J. Meijer, A. Luch, A. F. Thunemann and A. Lampen, Impact of an artificial digestion procedure on aluminum-containing nanomaterials, *Langmuir*, 2017, **33**, 10726–10735.
- E. Shaji, M. Santosh, K. V. Sarath, P. Prakash, V. Deepchand and B. V. Divya, Arsenic contamination of groundwater: A global synopsis with focus on the Indian Peninsula, *Geosci. Front.*, 2021, **12**, 101079.
- S. Fendorf, A. Michael Holly and A. van Geen, Spatial and temporal variations of groundwater arsenic in South and Southeast Asia, *Science*, 2010, **328**, 1123–1127.



- 28 X. Bi, C. Zeng and P. Westerhoff, Adsorption of arsenic ions transforms surface reactivity of engineered cerium oxide nanoparticles, *Environ. Sci. Technol.*, 2020, **54**, 9437–9444.
- 29 C. W. Neil, X. Wu, D. Kim, H. Jung, Y. Zhu, J. R. Ray and Y.-S. Jun, Arsenite oxyanions affect CeO<sub>2</sub> nanoparticle dissolution and colloidal stability, *Environ. Sci.: Nano*, 2021, **8**, 233–244.
- 30 Z. Mortazavi Milani, F. Charbgoon and M. Darroudi, Impact of physicochemical properties of cerium oxide nanoparticles on their toxicity effects, *Ceram. Int.*, 2017, **43**, 14572–14581.
- 31 J. Li, Y. Guo, X. Duan and B. Li, Tissue- and region-specific accumulation of arsenic species, especially in the brain of mice, after long-term arsenite exposure in drinking water, *Biol. Trace Elem. Res.*, 2020, **198**, 168–176.
- 32 J. Li, X. Duan, D. Dong, Y. Zhang, L. Zhao, W. Li, J. Chen, G. Sun and B. Li, Tissue-specific distributions of inorganic arsenic and its methylated metabolites, especially in cerebral cortex, cerebellum and hippocampus of mice after a single oral administration of arsenite, *J. Trace Elem. Med. Biol.*, 2017, **43**, 15–22.
- 33 A. E. Geiszinger, W. Goessler and K. A. Francesconi, The marine polychaete *Arenicola marina*: its unusual arsenic compound pattern and its uptake of arsenate from seawater, *Mar. Environ. Res.*, 2002, **53**, 37–50.
- 34 M. Vahter, Mechanisms of arsenic biotransformation, *Toxicology*, 2002, **181–182**, 211–217.
- 35 J. Wang, W. Hu, H. Yang, F. Chen, Y. Shu, G. Zhang, J. Liu, Y. Liu, H. Li and L. Guo, Arsenic concentrations, diversity and co-occurrence patterns of bacterial and fungal communities in the feces of mice under sub-chronic arsenic exposure through food, *Environ. Int.*, 2020, **138**, 105600.
- 36 L. Laloux, D. Kastrati, S. Cambier, A. C. Gutleb and Y. J. Schneider, The food Matrix and the gastrointestinal fluids alter the features of silver nanoparticle, *Small*, 2020, **16**, e1907687.
- 37 Z. Wang, C. Li, Y. Mu, Z. Lin, A. Yi, Q. Zhang and B. Yan, Nanoadduct relieves: Alleviation of developmental toxicity of Cr(VI) due to its spontaneous adsorption to Mg(OH)<sub>2</sub> nanoflakes, *J. Hazard. Mater.*, 2015, **287**, 296–305.
- 38 S. Guo, Y. Liang, L. Liu, M. Yin, A. Wang, K. Sun, Y. Li and Y. Shi, Research on the fate of polymeric nanoparticles in the process of the intestinal absorption based on model nanoparticles with various characteristics: size, surface charge and pro-hydrophobics, *J. Nanobiotechnol.*, 2021, **19**, 32.
- 39 F. Rosario, M. J. Bessa, F. Brandao, C. Costa, C. B. Lopes, A. C. Estrada, D. S. Tavares, J. P. Teixeira and A. T. Reis, Unravelling the potential cytotoxic effects of metal oxide nanoparticles and metal(Loid) mixtures on A549 human cell line, *Nanomaterials*, 2020, **10**, 447.
- 40 C. Zeng, C. Nguyen, S. Boitano, J. A. Field, F. Shadman and R. Sierra-Alvarez, Cerium dioxide (CeO<sub>2</sub>) nanoparticles decrease arsenite (As(III)) cytotoxicity to 16HBE14o- human bronchial epithelial cells, *Environ. Res.*, 2018, **164**, 452–458.
- 41 L. Feng, X. Yang, Y. Shi, S. Liang, T. Zhao, J. Duan and Z. Sun, Co-exposure subacute toxicity of silica nanoparticles and lead acetate on cardiovascular system, *Int. J. Nanomed.*, 2018, **13**, 7819–7834.
- 42 G. Pulido-Reyes, I. Rodea-Palomares, S. Das, T. S. Sakthivel, F. Leganes, R. Rosal, S. Seal and F. Fernandez-Pinas, Untangling the biological effects of cerium oxide nanoparticles: the role of surface valence states, *Sci. Rep.*, 2015, **5**, 15613.
- 43 S. Singh, T. Dosani, A. S. Karakoti, A. Kumar, S. Seal and W. T. Self, A phosphate-dependent shift in redox state of cerium oxide nanoparticles and its effects on catalytic properties, *Biomaterials*, 2011, **32**, 6745–6753.

